

Liquid-Liquid Phase Transitions in Silicon

M. W. C. Dharma-wardana^{✉*} and Dennis D. Klug[†]
National Research Council of Canada, Ottawa K1A 0R6, CanadaRichard C. Remsing[✉]
Rutgers University, Department of Chemistry and Chemical Biology, Piscataway, New Jersey 08854-8019 USA (Received 18 April 2020; accepted 17 July 2020; published 11 August 2020)

We use computationally simple neutral pseudoatom (“average atom”) density functional theory (DFT) and standard DFT to elucidate liquid-liquid phase transitions (LPTs) in liquid silicon. An ionization-driven transition and three LPTs including the known LPT near 2.5 g/cm^3 are found. They are robust even to 1 eV. The pair distribution functions, pair potentials, electrical conductivities, and compressibilities are reported. The LPTs are elucidated within a Fermi liquid picture of electron scattering at the Fermi energy that complements the transient covalent bonding picture.

DOI: 10.1103/PhysRevLett.125.075702

Introduction.—Light elements like C, Si, P etc., are insulators or semiconductors that become dense metals when molten. They manifest transient covalent binding (*tr-cb*) even after melting [1–5]. Warm-dense matter (WDM) techniques [6,7] can be used to study these materials over a broad density ($\bar{\rho}$) and temperature (T) range [8]. A recent study of WDM carbon provided pair-distribution functions (PDFs) $g(r)$ and other data suggestive of a phase transition from a highly correlated WDM state to a weakly correlated plasma, driven by a change in ionization [5]. The *supercooled* liquid silicon (*l*-Si) near 1200 K, polymorphic forms of silicon, as well as model fluids have been studied for a liquid-liquid phase transition (LPT) between a high-density liquid (HDL) and a low-density liquid (LDL) [9–18]. Remsing *et al.* [19,20] confirmed the LPT via density functional theory (DFT) based molecular dynamics (MD) for *l*-Si, using the “strongly constrained and appropriately normed” (SCAN) XC-functional [21] suitable for *tr-cb* systems. The nonmetallic LDL (*nm*-LDL) is less dense than the solid. Here we examine Si over a range of $\bar{\rho}$, T and find three LPTs viz., LPT2 near 2 g/cm^3 , LPT2.5 near $2.27\text{--}2.57 \text{ g/cm}^3$, LPT3 near 3 g/cm^3 , and an ionization-driven transition (IDT) at 1.5 g/cm^3 . The IDT and the LPTs are found to be robust and may be studied even at higher T .

Method.—We use standard N -center DFT-MD [22] and one-center neutral pseudoatom (NPA) methods [23–25]. The NPA reduces *both* the electron-electron and ion-ion many-body problems to two coupled one body problems via exchange-correlation functionals [26–32]. The NPA and the hyper-netted-chain (HNC) equation provide rapid, DFT results via mere “laptop” calculations for $g(r)$, the structure factor $S(k)$, and thermodynamic and transport properties (see the Supplemental Material [33]).

Phase transitions.—In DFT-MD the free energy $F(\bar{\rho}, T)$ is calculated using an N -atom simulation cell, with

$N \sim 100\text{--}500$. The NPA uses $N = 1$ and inputs the free electron density \bar{n} and T to construct the equilibrium ionic density $\bar{\rho}$, the mean ionic charge \bar{Z} (see [26,29,31,34,35]), ion-electron and ion-ion pair potentials. The free energies and linear transport properties (e.g., conductivity σ [36,37]) are obtained using only NPA-generated quantities [29,33]. In DFT-MD, the Kubo-Greenwood (KG) dynamic conductivity $\sigma(\omega)$ is calculated and averaged over many fixed ion configurations [38–40]. A mean-free path and a Drude model are invoked by KG to get the static KG conductivity $\sigma(\omega \rightarrow 0)$.

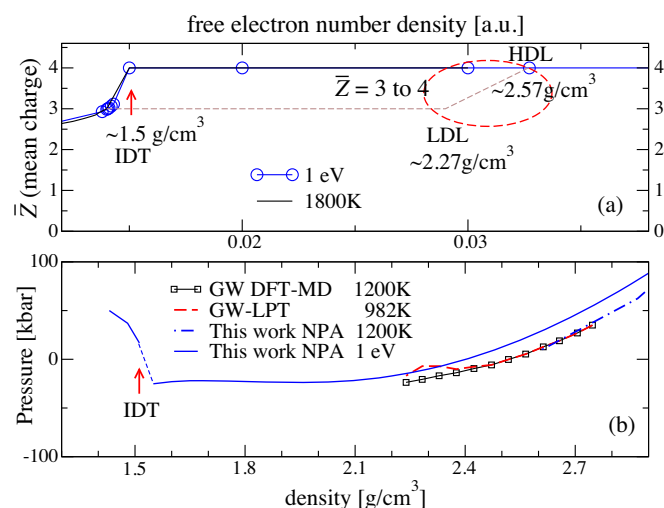


FIG. 1. (a) The Si charge \bar{Z} versus the free electron density n_f . At low density, a drop in \bar{Z} may cause an ionization driven transition (IDT). The ellipse indicates the HDL-LDL LPT. (b) The HDL branch of the Ganesh-Widom (GW) pressure [16] and the NPA at 1200 K agree. The pressure at 1 eV (11 604 K) is discontinuous at the IDT.

Several mechanisms for phase transitions in l -Si exist. (1) In l -Si ($\bar{\rho} = 2.56 \text{ g/cm}^3$) near the melting point (1683K), \bar{Z} is four. On lowering $\bar{\rho}$ sufficiently, \bar{Z} drops, and phase transitions may occur (Fig. 1). The transition of \bar{Z} from 4 to 3 occurs at $\rho < 1.5 \text{ g/cm}^3$ for l -Si at 1200 K. Such wide ranging $\bar{\rho}, T$ studies cannot be done using model potentials (e.g., Stillinger-Weber) [41] as the role of the electron quantum fluid is suppressed.

(2) If the first peak of $S(k)$ for some density range falls near $2k_F$ in a metallic fluid (as in l -Si), then concerted scattering across the Fermi surface causes a giant Kohn anomaly that translates into tr - cb with lifetimes typical of phonon vibrations [3]. That is the ‘‘Fermi liquid’’ picture of tr - cb formation. The presence of tr - cb splits the main peak of $S(k)$ and causes a peak in the PDF close to the Si-Si bond distance r_b .

(3) In simple metallic fluids, e.g., l -Al, the first peak of $g(r)$ occurs near $r_1 \sim 1.6r_{ws}$, where the Wigner-Seitz radius r_{ws} is $\{3/(4\pi\bar{\rho})\}^{1/3}$. This is a hard-sphere packing effect acting against the electron cohesive energy. Complex fluids can lower F further if $\bar{\rho}$ adjusts via an LPT to bring r_1 near $r_b \sim 2.1\text{--}2.5 \text{ \AA}$ for l -Si, and $\sim 1.5 \text{ \AA}$ for l -C. Transient bonding increases the available configurations and entropy, lowering F to drive the LPT [41].

The total free energy $F = F_e + F_i + F_{emb} + F_{12}$, is discussed in the Supplemental Material [33]. The F_{12} term contains ion-ion bonding effects. Its discontinuities indicate LPTs. The other terms vary fairly smoothly with density. Figure 2 displays $F_{12}(\bar{\rho})$ for l -Si at 1200 K. Similar (weaker) discontinuities are found even at $T = 1 \text{ eV}$ (see the Supplemental Material). The spherically symmetric model used allows only uniform-density solutions. In the following, and in the Supplemental Material, we discuss the

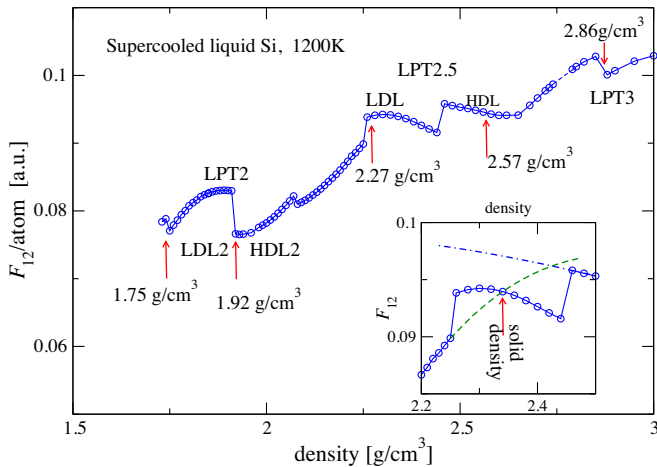


FIG. 2. The ion-ion part of the free energy F_{12} shows discontinuities at possible LPTs. The LPT2.5 at $2.27 \leq \bar{\rho} \leq 2.57 \text{ g/cm}^3$ is well known, while the LPT2, near $1.75\text{--}2 \text{ g/cm}^3$ and LPT3 near $1.78\text{--}3 \text{ g/cm}^3$ are proposed. The inset shows metastable extensions of F_{12} branches into the LPT2.5 region. DFT-MD finds a nonmetallic LDL in this region.

nature of the LPTs, their PDFs, the compressibility κ_T and the electrical conductivity σ across them. Optical probes can access σ and provide evidence for their onset.

Discussion of structure data.—The average charge state of the ion, i.e., \bar{Z} , is indirectly accessible from N -center DFT-MD simulations. It can be measured via the optical conductivity, x-ray Thomson scattering [42], or via Langmuir probes. In a mixture of charge states, \bar{Z} is the mean value over the composition fractions x_j of the integral charge states Z_j [29]. This is the case for $\bar{\rho} < 1.5 \text{ g/cm}^3$ when Z_j may be 4, 3, and 2 (see Fig. 1).

Figure 1 displays \bar{Z} versus the free electron density $n_f = \bar{n}$. The IDT and the pressure are further discussed in [33]. As the NPA-HNC converges poorly near the IDT at 1200 K, the $1 \text{ eV } P$ isotherm is given. At 1200 K we recover the Ganesh-Widom HDL pressure [16] extended up to LPT3. The PDFs at the IDT (discussed in [33]) show short Si-Si tr - cb s with r_b of $\sim 2.13 \text{ \AA}$ compared to r_b in LDL-Si near $2.27\text{--}2.29 \text{ g/cm}^3$ at 1200 K. Near the IDT the Si-Si r_b is 9% shorter than in the solid, with stronger bonding due to weaker screening for $\bar{Z} = 3$.

Figure 3 displays the variation of the l -Si $S(k)$ at 1200 K, for $\bar{\rho}$ at 2.57 g/cm^3 (HDL), through the LPT2.5 to 2.27 g/cm^3 (LDL) and to 1.9 g/cm^3 at the LPT2. The major peak in $S(k)$ is found to be at $\sim 2k_F$ as expected from the FLP, with a subsidiary peak in the low- k region. At 1.47 g/cm^3 , beyond the IDT (inset, Fig. 3), $\bar{Z} = 3$ and no $2k_F$ splitting exists. When transient bonding occurs, the valence \bar{Z} , a static average, does not change. Instead, the self-energy correction from $2k_F$ scattering produces an increased electron-effective mass m^* [3,43–45], with

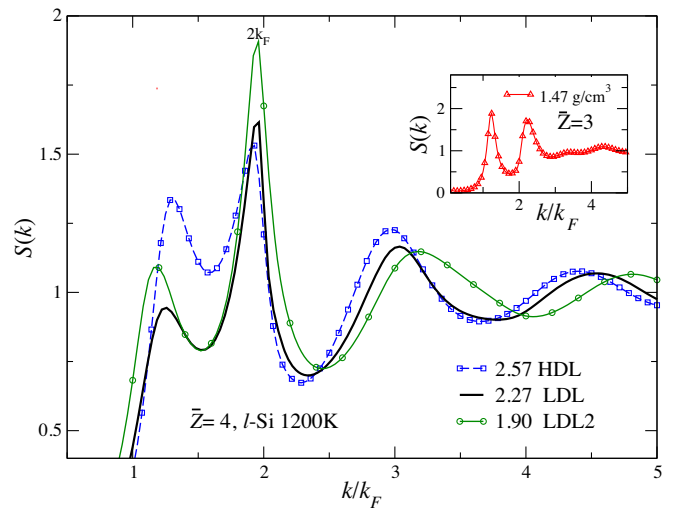


FIG. 3. The structure factor $S(k)$ of LPT2.5 and LPT2 at 1200 K. The main split-off-peak registers at $2k_F$ as required by the Fermi liquid picture (this holds for LPT3 also, though not displayed). The x axis is k/k_F with k_F appropriate to $\bar{Z} = 4$. The inset for $S(k)$ at 1.47 g/cm^3 , $\bar{Z} = 3$, is beyond the IDT, and shows no $2k_F$ splitting.

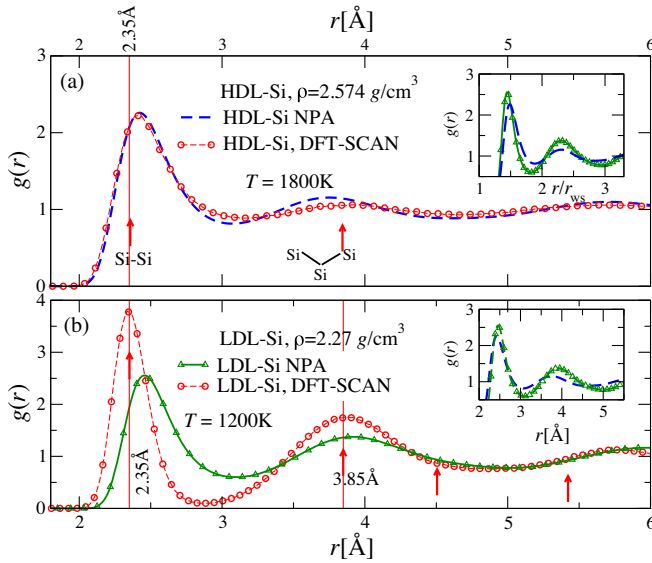


FIG. 4. $g(r)$ of (a) HDL (2.57 g/cm^3) Si from NPA and from DFT-SCAN at 1800 K, (b) LDL ($\sim 2.27 \text{ g/cm}^3$) Si from NPA and DFT-SCAN. The Si-Si bond length (2.35 \AA) is indicated. The NPA-HNC fails to capture the increased $g(r)$ at 2.35 \AA and remain locked in an HDL-like structure. Insets: the NPA $g(r)$, for HDL-Si and LDL-Si versus r/r_{ws} , and with r in \AA . The HDL $r_{\text{ws}} \simeq 3 \text{ a.u.}$

$m^* \simeq 1.1$ [46]. If $m^* = 1$ the double peaks of $S(k)$ become a single peak at $2k_F$ (see [33]). This links the experimentally observed split peak [47], *tr-cbs*, and the LPT with $2k_F$ scattering.

The PDFs for the LDL and HDL reported in Ref. [20] are displayed in Fig. 4 while their $S(k)$ are displayed in the Supplemental Material [33]. Figure 4(a) shows the first peak of the NPA $g(r)$ at 2.43 \AA . This is not determined by packing effects but by *tr-cb*. A hard-sphere bridge term to the HNC equation via the Lado-Foils-Ashcroft (LFA) criterion [48] returns a negligible correction, as with *l-C* and *l-Ge*. The HDL and LDL $g(r)$ show a sharp peak near 2.45 \AA some 4% larger than the nominal Si-Si r_b in the solid. The higher electron density in the liquid weakens the Si-Si interaction and leads to a longer average *tr-cb*.

The higher- r peaks in the $g(r)$ of the HDL from DFT-SCAN studies and from the NPA agree well, both for peak position and height. As discussed in the Supplemental Material [33], both $S(k)$ and $g(r)$ for HDL-Si from DFT-SCAN agree with NPA results, exhibiting the split-structure of the first subpeak of $S(k)$, while the higher- k subpeak falls at $\sim 2k_F$. The low- k subpeak at $\sim 2 \text{ \AA}^{-1}$ registers with the low- k structure in the crystal $S(k)$, especially for the DFT-SCAN result for LDL-Si at 1200 K.

In contrast, in Fig. 4(b), the $g(r)$ for LDL-Si obtained from NPA and from DFT-SCAN differ. A massive, wide first peak at the Si nearest-neighbor (NN) position is observed in DFT-SCAN, with the second peak squarely at the Si next-NN position. The NPA calculation for

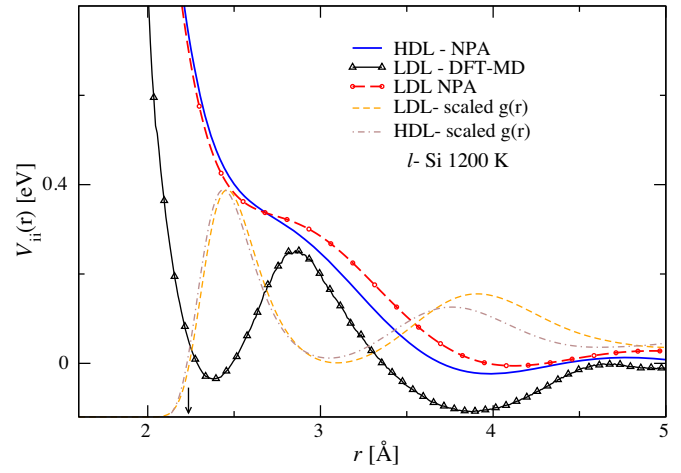


FIG. 5. The ion-ion potentials of the HDL and LDL are shown against their PDFs (scaled to match the potentials). The arrow at r_b marks the Si-Si bond length. The first shell of ions sits on a repulsive ledge stabilized by the electron cohesive energy, while the second shell is in a Friedel-oscillation minimum (FOM). The HDL \rightarrow LDL involves a cooperative movement of ions to the second shell as seen in the enhanced LDL $g(r)$ in the FOM region. This picture holds also for the LPT2 and LPT3 (see [33]). The DFT-SCAN potential accommodates the first shell at its true minimum.

LDL-Si returns a $g(r)$ only slightly modified from HDL-Si at 1800 K, as seen in the two insets, where the NPA $g(r)$ for the HDL and LDL at 1800 and 1200 K are compared. The NPA-LDL is a metallic liquid, while the LDL of DFT-SCAN is nonmetallic (see conductivity).

To understand the temperature-robust LPTs found via the NPA, and the metastable LDL found so far via DFT-SCAN, we look at pair-potentials in relation to their PDFs (Fig. 5). The figure implies a first shell of ions on a positive-energy ledge as also found in liquid-aluminum [3,43]. These LDLs of NPA-HNC are distinct phases separated from the HDLs by free-energy jumps. With the coordination number $N_c = 6$ at the LPT2.5, the densities at LPT2 and LPT3 correspond to $N_c = 5$ and 7. One may expect similar transitions at higher densities, until $N_c = 12$ in a high density solid form. The transitions are cooperative because the Fermi length ($1/k_F$) is tied to the density via the peak of $S(k)$. The HDL-LDL transition to *nm*-LDL found in DFT-MD is likely to be $N_c = 6 \rightarrow 5$ and 4. The metallic LDLs may be stable precursors of metastable low- T *nm*-LDLs, as seen at LPT2.5, and likely to be seen at LPT2 as well. The inset to Fig. 2 shows metastable extensions of F_{12} near the solid density. N -atom simulations that emphasize bonding and solidlike boundary conditions succeed in detecting an *nm*-LDL below the solid density here and are sensitive to XC functionals [21,49].

Conductivity.—The static electrical conductivity $\sigma = \sigma(\omega = 0)$ is measurable by “older” methods and via laser pump-probe techniques. In the degenerate regime

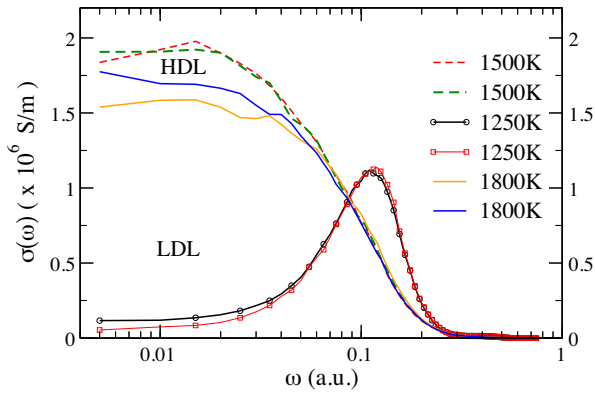


FIG. 6. $\sigma(\omega)$ from DFT-MG-KG. for HDL and LDL Si at LPT2.5. The LDL has a striking finite $\sigma(\omega)$, but the static σ indicates a nearly nonmetallic LDL.

($T \ll E_F$), electron scattering is mostly from $-k_F$ to $+k_F$, with a momentum transfer of $q \simeq 2k_F$. Even at the highest T studied here (1 eV), the electrons in l -Si are strongly degenerate as $T/E_F \sim 0.078$ prior to the IDT. As T increases, σ decreases essentially linearly for metals, though not so in l -Si data. This is reflected in our NPA-Ziman results given in [33]. DFT-KG calculations yield a dynamic conductivity $\sigma(\omega)$ averaged over fixed configurations. Figure 6 shows $\sigma(\omega)$ from typical DFT-KG calculations. The difference in the HDL and LDL $\sigma(\omega)$ is striking. For $\omega < \omega(\sigma_{\max}) \simeq 3$ eV, the electrons seem to be in localized states of what may be a “mobility edge” of LDL-Si. In HDL tr - cb the static limit $\omega \rightarrow 0$ is metallic.

Figure 7 indicates that DFT-SCAN estimates of $\bar{\rho}(T)$ agree well with the experimental data of Zhou *et al.* [50], but less so with Sasaki *et al.* [51]. Even when the density agrees, the $\sigma(0)$ from DFT-KG (Fig. 6) or the NPA-Ziman (Fig. 7) are only in partial agreement with experiments.

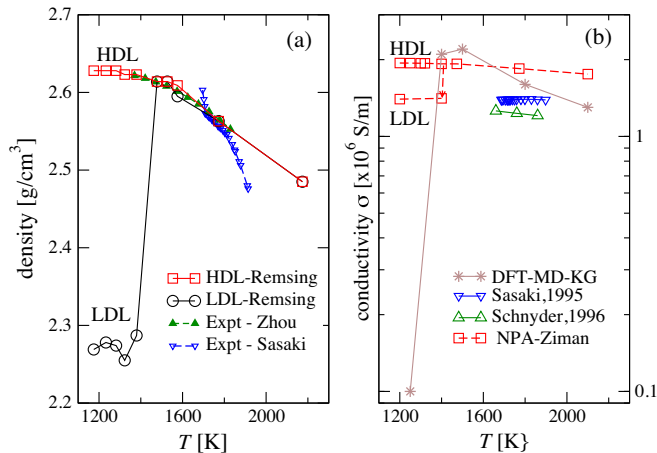


FIG. 7. (a) The density $\bar{\rho}$ versus T from DFT-SCAN [20] near LPT2.5 is compared with available experimental densities. (b) The static conductivity σ from NPA-Ziman, DFT-KG and from experiments [51,52].

Finite- T σ data at 1 eV are given in the Supplemental Material [33]. The NPA treats l -Si as a single fluid whereas many structures and a distribution of m^* may be needed to estimate σ .

The IDT and critical-point models.—Discussions of the HDL-LDL phases in tetrahedral fluids have used a critical-point free model [53], models with a liquid-liquid critical point [41], and models with two measures of order [54]. The electron fluid and the FLP have not figured much in these discussions inspired from theories on nonmetallic liquids like water. The LPTs found in this study are most easily understood within the FLP.

Conclusion.—Liquid Si shows three liquid-liquid phase transitions and possibly an ionization-driven transition changing $\bar{Z} = 4$ to 3 in the density range 1.5–3 g/cm³. The LPTs are linked to the splitting of the main peak of the structure factor by concerted electron scattering at the Fermi energy. The LPTs are robust and are seen (though weakened) even at 1 eV. While the HDL near 2.5 g/cm³ found in this study agrees with previous DFT-MD studies, the LDLs found via the NPA-HNC are stable metallic liquids that may be precursors to metastable nonmetallic LDLs found in supercooled liquid Si near 2.27 g/cm³. The HDL and LDL conductivities differ sufficiently and may provide an experimental signature of the LPTs in optical and conductivity experiments [12]. The compressibility (see [33]) displays robust signatures of the LPTs, but they need to be confirmed by refined shock-Hugoniot type experiments. At densities 1.5 g/cm³ the free electron density is reduced by localizing electrons into the atomic core, leading to a possible IDT.

*chandre.dharma-wardana@nrc-cnrc.gc.ca

†dennis.klug@nrc-cnrc.gc.ca

- [1] L. I. Aptekar, Dokl. Akad. Nauk SSSR **249**, 1099 (1979) [Sov. Phys. Dokl. **24**, 993 (1979)].
- [2] I. Štich, R. Car, and M. Parrinello, *Phys. Rev. Lett.* **63**, 2240 (1989).
- [3] M. W. C. Dharma-wardana and F. Perrot, *Phys. Rev. Lett.* **65**, 76 (1990).
- [4] J. T. Okada, P. H.-L. Sit, Y. Watanabe, Y. J. Wang, B. Barbiellini, T. Ishikawa *et al.*, *Phys. Rev. Lett.* **108**, 067402 (2012).
- [5] M. W. C. Dharma-wardana, *Contrib. Plasma Phys.* **58**, 128 (2018).
- [6] E. E. McBride, A. Krygier, A. Ehnes, E. Galtier, M. Harmand, Z. Konôpková *et al.*, *Nat. Phys.* **15**, 89 (2019).
- [7] A. Ng, T. Ao, F. Perrot, M. W. C. Dharma-wardana, and M. E. Foord, *Laser Part. Beams* **23**, 527 (2005).
- [8] S. X. Hu, R. Gao, Y. Ding, L. A. Collins, and J. D. Kress, *Phys. Rev. E* **95**, 043210 (2017).
- [9] S. Sastry and C. A. Angell, *Nat. Mater.* **2**, 739 (2003).
- [10] S. S. Ashwin, U. V. Waghmare, and S. Sastry, *Phys. Rev. Lett.* **92**, 175701 (2004).
- [11] T. Morishita, *Phys. Rev. Lett.* **93**, 055503 (2004).

- [12] P. F. McMillan, M. Wilson, D. Daisenberger, and D. Machon, *Nat. Mater.* **4**, 680 (2005).
- [13] T. Morishita, *Phys. Rev. Lett.* **97**, 165502 (2006).
- [14] P. Beaucage and N. Mousseau, *J. Phys. Condens. Matter* **17**, 2269 (2005).
- [15] D. Daisenberger, M. Wilson, P. F. McMillan, R. Q. Cabrera, M. C. Wilding, and D. Machon, *Phys. Rev. B* **75**, 224118 (2007).
- [16] P. Ganesh and M. Widom, *Phys. Rev. Lett.* **102**, 075701 (2009).
- [17] M. Beye, F. Sorgenfrei, W. F. Schlotter, W. Wurth, and A. Föhlisch, *Proc. Natl. Acad. Sci. U.S.A.* **107**, 16772 (2010).
- [18] V. V. Vasisht, S. Saw, and S. Sastry, *Nat. Phys.* **7**, 549 (2011).
- [19] R. C. Remsing, M. L. Klein, and J. Sun, *Phys. Rev. B* **96**, 024203 (2017).
- [20] R. C. Remsing, M. L. Klein, and J. Sun, *Phys. Rev. B* **97**, 140103(R) (2018).
- [21] J. Sun, B. Xiao, Y. Fang, R. Haunschild, P. Hao, A. Ruzsinszky, G. I. Csonka, G. E. Scuseria, and J. P. Perdew, *Phys. Rev. Lett.* **111**, 106401 (2013).
- [22] VASP-Vienna ab-initio simulation package: G. Kress, J. Furthmüller, and J. Hafner, <http://cms.mpi.univie.ac.at/vasp/>; ABINIT: X. Gonze, B. Amadon, P.-M. Anglade *et al.*, *Comput. Phys. Commun.* **180**, 2582 (2009).
- [23] M. W. C. Dharma-wardana, *Contrib. Plasma Phys.* **55**, 79 (2015).
- [24] L. Harbour, M. W. C. Dharma-wardana, D. D. Klug, and L. J. Lewis, *Phys. Rev. E* **94**, 053211 (2016).
- [25] L. Harbour, G. D. Förster, M. W. C. Dharma-wardana, and L. J. Lewis, *Phys. Rev. E* **97**, 043210 (2018).
- [26] M. W. C. Dharma-wardana and F. Perrot, *Phys. Rev. A* **26**, 2096 (1982).
- [27] F. Perrot, *Phys. Rev. E* **47**, 570 (1993).
- [28] E. K. U. Gross and R. M. Dreizler, in *Density Functional Theory*, NATO ASI Series Vol. 337 (Plenum Press, New York, 1993), p. 625.
- [29] F. Perrot and M. W. C. Dharma-wardana, *Phys. Rev. E* **52**, 5352 (1995).
- [30] F. Perrot and M. W. C. Dharma-wardana, *Phys. Rev. B* **62**, 16536 (2000); **67**, 079901 (2003).
- [31] M. S. Murillo, J. Weisheit, S. B. Hansen, and M. W. C. Dharma-wardana, *Phys. Rev. E* **87**, 063113 (2013).
- [32] M. W. C. Dharma-wardana, *Phys. Rev. B* **100**, 155143 (2019).
- [33] See the Supplemental Material at <http://link.aps.org/supplemental/10.1103/PhysRevLett.125.075702> for details of the NPA method, Free energy discontinuities, compressibility at 1 eV, conductivities. More details of PDFs, pair-potentials, and m^* , and the nature of the liquid-liquid phase transitions are given.
- [34] R. M. More, *Adv. At. Mol. Phys.* **21**, 306 (1985).
- [35] P. A. Sterne, S. B. Hansen, B. G. Wilson, and W. A. Isaacs, *High Energy Density Phys.* **3**, 278 (2007).
- [36] M. W. C. Dharma-wardana, D. D. Klug, L. Harbour, and L. J. Lewis, *Phys. Rev. E* **96**, 053206 (2017).
- [37] P. L. Rossiter, *The Electrical Resistivity of Metals and Alloys* (Cambridge University Press, Cambridge, UK, 1987).
- [38] V. Recoules, P. Renaudin, J. Clérrouin, P. Noiret, and G. Zérah, *Phys. Rev. E* **66**, 056412 (2002).
- [39] M. Pozzo, M. P. Desjarlais, and D. Alfè, *Phys. Rev. B* **84**, 054203 (2011).
- [40] K. P. Migdal, V. V. Zhakhovsky, A. V. Yanilkin, Yu. V. Petrov, and N. A. Inogamov, *Appl. Surf. Sci.* **478**, 818 (2019).
- [41] G. Zhao, J. L. Yan, Y. J. Yu, M. C. Ding, X. G. Zhao, and H. Y. Wang, *Sci. Rep.* **7**, 39952 (2017).
- [42] S. H. Glenzer and R. Redmer, *Rev. Mod. Phys.* **81**, 1625 (2009).
- [43] M. W. C. Dharma-wardana and G. C. Aers, *Phys. Rev. B* **28**, 1701 (1983).
- [44] M. Itoh and M. Watabe, *J. Phys. F* **14**, L9 (1984).
- [45] N. H. March, *Can. J. Phys.* **65**, 219 (1987).
- [46] M. W. C. Dharma-wardana, *Phys. Rev. E* **86**, 036407 (2012).
- [47] Y. Waseda, *Structure of Non-crystalline Materials* (McGraw-Hill, New York, 1980).
- [48] F. Lado, S. M. Foiles, and N. W. Ashcroft, *Phys. Rev. A* **28**, 2374 (1983).
- [49] W. Kohn, *Phys. Rev. B* **33**, 4331(R) (1986).
- [50] Z. Zhou, S. Mukherjee, and W.-K. Rhim, *J. Cryst. Growth* **257**, 350 (2003).
- [51] H. Sasaki, A. Ikari, K. Terashima, and S. Kimura, *Jpn. J. Appl. Phys.* **34**, 3426 (1995).
- [52] H. S. Schnyders and J. B. Van Zytveld, *J. Phys. Condens. Matter* **8**, 10875 (1996).
- [53] C. A. Angell, *Nat. Mater.* **13**, 673 (2014).
- [54] J. R. Errington and P. G. Debenedetti, *Nature (London)* **409**, 318 (2001).